RSC Advances

ROYAL SOCIETY OF CHEMISTRY

www.rsc.org/advances

Table of content:

Title:Investigation on Regeneration Kinetics of Organic Dyes with Pyridine Ring Anchoring Group by Scanning Electrochemical Microscopy

Author: Getachew Alemu, Jin Cui, Kun Cao, Junpeng Li, Yan Shen* and Mingkui Wang*

The regeneration dynamics can be understood with the help of scanning electrochemical microscopy, showing that anchoring group significantly affects the effective rate constant.

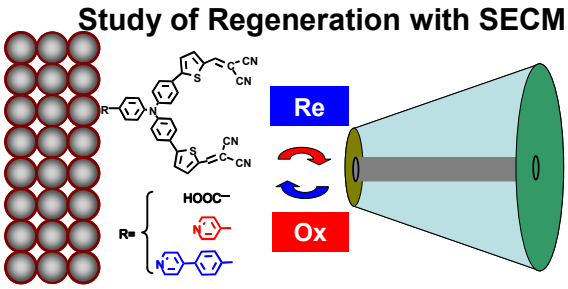

Cite this: DOI: 10.1039/c0xx00000x

www.rsc.org/xxxxxx

ARTICLE TYPE

Investigation on Regeneration Kinetics of Organic Dyes with Pyridine Ring Anchoring Group by Scanning Electrochemical Microscopy

Getachew Alemu, Jin Cui, Kun Cao, Junpeng Li, Yan Shen* and Mingkui Wang*

Received (in XXX, XXX) Xth XXXXXXXXX 20XX, Accepted Xth XXXXXXXXX 20XX
DOI: 10.1039/b000000x

This work reports on a study of regeneration kinetics of organic dyes with pyridine ring group sensitized NiO electrode in combination with iodide-based and organic thiolate-based electrolytes by scanning electrochemical microscopy (SCEM) with feedback model. These dyes have showed promising performance in p-type dye-sensitized solar cells. The investigation reveals that the anchoring group affects the effective rate constant, showing that an efficient dye-regeneration process for the dye with carboxylic acid anchoring group. Meanwhile, it is worthy to note that the regeneration process between the reduced dye and oxidized state of thiolate-based electrolyte is much faster than that of iodide-based electrolyte.

Introduction

The worldwide demand for energy is expected to be double by the next decade. An abundant supply of energy is necessary for global political, economic and environmental stability.[1-4] Recently, third generation photovoltaic technology, including nanocrystal solar cell and organic solar cell, has attracted much attention due to low cost, simple fabrication relative to others.[5,6] Mesoscopic solar cells offer credible and attractive alternative to solid-state p-n junction devices, which efficient transfer solar energy to storable energy based on photosynthesis. For example, dye-sensitized solar cells (DSSC) are under intensive investigation, the promising solution to future large-scale energy conversion issues. Conventional DSSCs typically contain several components such as mesoporous semiconductor metal oxide film, sensitizer, electrolyte/hole conductor, and counter electrode.[7,8] An efficient DSSC device depends on several coupled processes.[2,9] Upon excitation, the sensitizer injects an electron and hole into the n- and the p-type selective contact materials, respectively, resulting in the photon-generated charge carriers in femtosecond time regime, which are collected at the front and back electrode of device. The photovoltage developed by the cell corresponds to the difference in the quasi-Fermi levels of the n- and the p-type selectove contact materials under illumination. It is significant that the positively charged oxidized/photo excited dye D^+ is restored to ground state D in nanosecond time regime by receiving an electron from the reduced specie electrolyte (usually being I^-).[9,10] Mesoporous solar cell configuration has great advantage because this solar energy conversion process involves only majority charge carriers.

To date, an optimum light to electrical energy conversion efficiency of 11.5% has been obtained for ruthenium complex-based DSSCs under reporting conditions with a liquid-junction device configuration.[11-13] Even higher efficiencies of 12.3-13% have recently been reported for DSSC with porphyrin sensitizers and cobalt-based mediators.[3,14] Therefore, it is critical to develop new dyes with properties of increased optical cross-section and capable of absorbing longer wavelengths. Other current research focuses on factors including nanomaterials and quantum dots aiming to boost the conversion efficiency. Recently, new type of DSSCs based on sensitization of p-type semiconductor (p-SC, typically NiO) have emerged with great interests.[15-18] Contrary to the conventional n-type DSSC, in p-type DSSC the photo-excited sensitizer is reductively quenched by hole injection into the valence band of p-SC.[18,19]

The efficiency of p-DSSC is intrinsically limited by low open circuit voltage (V_{OC}) and photocurrent. A low photovoltage could be caused by the small difference in potential between the quasi-Fermi level of p-SCs and the electrochemical equilibrium potential of redox mediators.[24] The low photocurrent could be related to fast charge recombination between the reduced dye and the holes generated in the NiO, as well as a low light-harvesting efficiency resulting from the limited dye loading on p-type SC film, which leads to low efficiencies.[20-23] The role of mediator is continuously to regenerate the reduced sensitizers after hole injection to p-SC valence band and

transport charges to the counter electrode. To promote regeneration, redox mediator should satisfy key properties, such fast electron self-exchange rate, and high diffusion coefficient to ensure fast transport of charges to counter electrodes. [23,24]

Dye regeneration is critical reaction in p-DSSC device, which must be faster than recombination process.[25-27] The regeneration kinetics of DSSC depends on various factors, including electrode materials, dye structure, electrolyte composition, and solvent viscosity, etc.[11,13,28] Currently, there are few techniques available to study dye-regeneration kinetics at the dye-sensitized nanocrystalline/ electrolyte interface in DSSC devices. These are transient adsorption spectroscopy and pump-probe spectroscopy fast incident irradiation.[29,30] Scanning electrochemical microscopy (SECM) has been widely used as an effective technique to determining electron transfer kinetics at various interfaces, including polymer/liquid,[31] liquid/liquid interfaces,[32] redox enzymes on solid supports,[33] and SC/electrolyte interfaces.[34,35] Recently, Wittstock *et al* successfully proposed using SECM to describe the kinetics of dye-regeneration in DSSCs.[36-38]

In this work, we report on SECM investigation of the influence of anchoring groups on dye-regeneration kinetics at dye-sensitized p-type NiO electrode/electrolyte interface. Specifically, organic sensitizers (P1, CW1, and CW2, see Figure 1),[39] in conjunction with thiolate- and iodide-based electrolytes were selected in order to compare the regeneration process. The regeneration kinetics was found to depend on the structure of the dye and the concentration of the redox couples, which affect the driving force for regeneration. This contributes to identify of appropriate electrolytes and design of effective sensitizers for highly efficient P-DSSCs.[40-42]

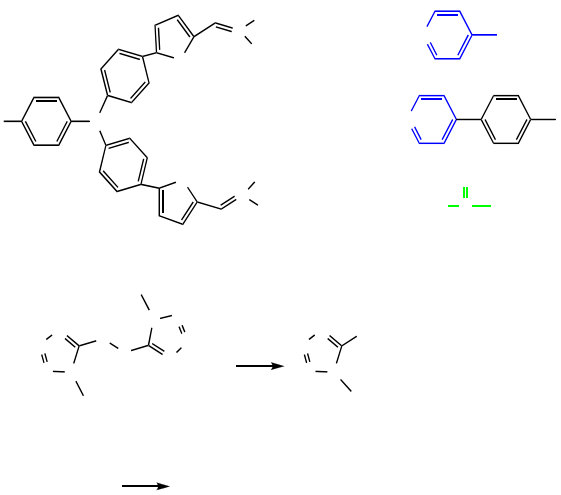

Fig. 1 The structure of dyes (CW1, CW2, and P1) and redox shuttles (thiolate-based and iodide-based electrolytes).

Experimental section

Chemicals

The sensitizer P1, CW1, CW2, and redox shuttles (Figure 1) were synthesized according to literatures.[39] lithium Bis (trifluoromethylsulfonyl) imide (LiTFSI) was used as supporting electrolyte. LiI solution was prepared by mixing in 1mM solution of LiI in acetonitrile with 0.1 M LiTFSI and diluting the resulting stock solution to the required concentration

Preparation of NiO/Dye film

The NiO nanoparticles paste was prepared as fellow 3 mg NiO of nanoparticles (particle size ~20 nm) were ball-milled in 80 mL ethanol overnight. Two kinds of ethyl cellulose (EC) i.e., EC (#5-15 mPas) and EC (#30-60 mPas) were used as binder. The mixture of NiO, EC, triponal, and ethanol was sonicated and stirred over night to obtain fine dispersion.[43-45] A paste was made by evaporating ethanol from the mixture with a rotary evaporator. FTO glass were coated with nickel acetate ethanol solution (0.05 M) by dip coating and subsequently dried in air. The photocathode films were screen-printed with the NiO paste and dried for 5 min at 125 ºC. This screen printing procedure was repeated to obtain films with different thickness.[43-45]

Instruments and procedures

SECM feed back mode experiments were performed on CHI 920C electrochemical workstation (CH Instruments, Shanghai). A homemade Teflon cell (with volume of 2 mL) was used to hold a Pt wire counter electrode, an Ag/Ag^+ reference electrode. The photocathodes FTO/NiO/organic dyes sample films were attached to the cell bottom and sealed with an O-ring as working electrode. In SECM measurements, the dye-sensitized transparent SC nanocrystal films (NiO with a thickness of about 2.3 µm) were used as the working electrode. An extra Pt wire was connected to FTO substrate with the electrolyte in order to operate the photoelectrochemical cell in a short-circuit setup. A12.5 µm radius Pt wire (Goodfellow, Cambridge, UK) was sealed into a 5 cm glass capillary prepared by a Vertical pull pin instrument (PC-10, Japan). The ultra-microelectrode (UME) was polished by a grinding instrument (EG-400, Japan) and micro-polishing cloth with 0.3 µm alumina powder. Then the UME was sharpened conically to a RG of 10, where RG is the ratio between the diameters of the glass sheath and the Pt disk. All experiments were carried out at room temperature. The irradiation was focused onto the backside of the photoanode from light emitting diode.[36,37]

Result and Discussion

In this study, scanning electrochemical microscopy (SCEM) with feedback model was used to analyse the effect of anchoring group on dye regeneration kinetics with various electrolytes under illumination. Two organic dyes with pyridine ring anchoring groups (CW1 and CW2) were synthesized as analogues of P1 dye to better understand the influence of the anchoring group on the regeneration parameters of their corresponding p-DSSCs.[39] As shown in Figure 1, the three dyes contain a common

triphenylamine electron-donating group, a single thiophene π-bridge and a 2,2-dicyano-vinyl electron-acceptor group. The CW1 and CW2 dyes contain a pyridine moiety, which acts as a weak electron-withdrawing group and has the same function as the carboxylic acid anchoring group in P1 dye. The introduction of a phenyl conjugate linker between the pyridine ring and the triphenylamine donor produces CW2 with a rigid structure and may stand it up on the NiO surface after dye adsorption, resulting in sufficient dye loading. The device with P1 dye showed photovoltaic efficiency of 0.143% with Voc of 92.9 mV, Jsc of 4.67 mA cm^{-2} and FF of 0.33. The device with dye CW1, which contains a pyridine moiety as the anchoring group, exhibited V_{OC} of 99 mV, Jsc of 2.66 mA cm^{-2}, and FF of 0.35, thus giving an overall PCE of 0.093%. The device with dye CW2, which contains a phenyl pyridine moiety as the anchoring group, exhibited V_{oc} of 118 mV, J_{sc} of 4.05 mA cm^{-2}, and FF of 0.34, giving an overall IPCE of 0.16%.[39]

Figure S1 in the supporting information presents the cyclic voltammetry of Pt UME in T^- and I^- mediator in acetonitrile, corresponding to the steady-state anodic waves according to Eq. 1. This measurement was performed in an electrochemical cell with P1 dye-sensitized NiO substrate. Therefore, the reaction on the UME couples with those on the substrate, which are expressed in Eq. 2.[36] It is evident that the steady state current for I^- oxidation varies dramatically compared to T^- with the same solvent and concentration. The tip currents for T^--based electrolyte exceeds four times more than I^--based electrolyte.

$$1.5I^- - e^- \rightarrow 0.5I_3^- \qquad (1a)$$

$$T^- - 2e^- \rightarrow T_2 \qquad (1b)$$

$$2D^-/NiO + I_3^- \rightarrow 2D/NiO + 3I^- \qquad (2a)$$

$$2D^-/NiO + T_2 \rightarrow 2D/NiO + 2T^- \qquad (2b)$$

In SECM feedback mode under short-circuit condition, the oxidized species of electrolytes (I^-_3 and T_2 in this study) were generated by an electrochemical reaction at UME (Eq. 1) and diffuses to dye-sensitized NiO electrode substrates. When the substrate is illuminated from the back, the reduced state of dye molecules (D^-) are regenerated by the oxidized species of redox shuttles accroding to Eq. 2, producing the reduced states of redox electrolytes, which eventually diffuse to the UME surface. This process leads to a full cycle reaction between the UME and dye-sensitized substrate. The SECM measurement records the current variations at the UME as a function of normalized distance L ($L=d/r_T$, d being the distance between the tip and the substrate, r_T being the radius of the Pt tip) between the UME and the surface of dye-ensitized NiO sample.

Generally, the normalized approach curve in the SECM feedback mode can be described by Eq. 3.

$$I_T(L) = I_T^{ins}(T) + \left(1 - \frac{I_T^{ins}(L)}{I_T^{cond}(L)}\right) I_S(L) \qquad (3)$$

where I_T^{cond} is the current for diffusion-controlled mediator recycling at the sample (positive feedback) and I_T^{ins} describes the current if no reaction occurs at the insulating sample (negative feedback), and $I_{S(L)}$ ($I_{S(L)} = I_S/I_{T,\infty}$) describes the current at the substrate electrode normalized by the current of the UME in the mediator solution (see supporting information).

From the mathematical description of the mass transport and kinetics at the surface of dye sensitized NiO sample, first-order rate constant κ can be extracted. Then, the effective heterogeneous rate constant k_{eff} can be evaluated with equation of $k_{eff}=\kappa D/r_T$, where D is the diffusion coefficient for the redox couple. The diffusion coefficients can be determined from microelectrode steady-state currents.[37] The typical values of diffusion coefficients are $D=1.86\times10^{-5}$ cm^2 s^{-1} for I^- electrolyte and $D=1.35\times10^{-5}$ cm^2 s^{-1} for T^- electrolyte, respectively. The reduction constant k_{red} for regeneration of excited dye by the oxidized state of redox shuttle in p-type DSSC device can be extracted from Eq. 4.[36]

$$k_{eff} = \frac{3[D]\varphi_{hv} j_{hv} k_{red}}{6k_{red}[C] + 2\varphi_{hv} J_{hv}} \qquad (4)$$

where [D] is the surface concentration of the dye in the ground state (mol cm^{-3}), k_{red} is the heterogeneous rate constant for the reduction of dye by electrolyte, [C] is the concentration of redox shuttle in electrolyte (mol cm^{-3}), l is the film thickness (cm), Φ_{hv} is the excitation cross-section of the adsorbed dye (cm^2 mol^{-1}), and J_{hv} is the incident photon flux density, respectively.

Figure 2a shows the normalized experimental approach curves and their corresponding fitting curves according to Eq. 3 upon approaching the UME (radius: 12.5 μm) to NiO/P1 film in 0.1 mM I^- solution under illumination with a blue LED at different illumination intensities. As the UME approaches the dye-sensitized substrate, the normalized tip current decreases, indicating that tip current depends on the kinetics of reverse reaction on the substrate. Also it was found higher feedback currents for higher light intensities, implying that regeneration rate increases with illumination intensities. When the film was back-illuminated, the current was significantly larger than in the dark (curve insulting surface curve#0). Under illumination photon density of blue LED changed from 2.2×10^9 to 22.4×10^9 mol cm^2 s^{-1}, their corresponding rate constants k_{eff} increased from 0.134×10^{-3} to 1.056×10^{-3} cm s^{-1}. In similar pattern, Figure 2b shows when photon density of red LED increased from 4.19×10^9 to 14.684×10^9 mol cm^2 s^{-1}, their corresponding rate constants k_{eff} incresed from 0.0178×10^{-3} to 0.2484×10^{-3} cm s^{-1}.

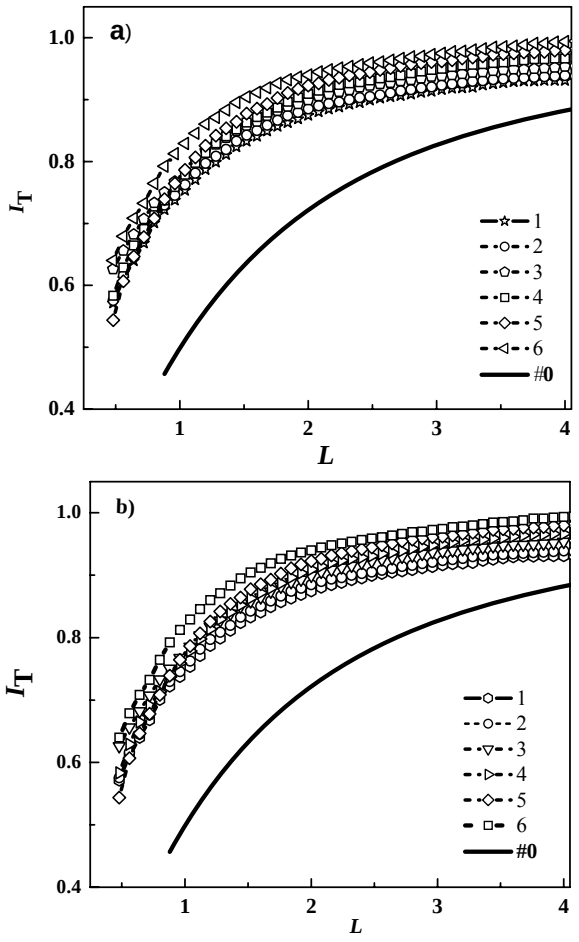

Fig. 2 (a) Comparison of normalized SECM approach curves for the approach of a Pt disk UME towards a NiO/P1 film in 1 mM I^- solution under different illumination. Photon flux density for (a) blue LED (in 10^{-9} mol cm^{-2} s^{-1}): (1) 2.2, (2) 6.1, (3)11.8, (4) 13.9, (5) 19.8, (6) 22.4. The first-order rate constant κ was estimated to be: (1) 0.009, (2) 0.013, (3) 0.025, (4) 0.036, (5) 0.05, (6) 0.099, and the effective rate constant k_{eff} (10^{-3} cm s^{-1}) was estimated to be: (1) 0.134, (2) 0.193, (3) 0.372, (4) 0.535, (5) 0.788, (6) 1.473, respectively; and for (b) red LED: (1) 4.19, (2) 6.81, (3) 9.44 (4) 12.06, (5) 13.11, (6) 14.68. The first-order rate constant k was estimated to be: (1) 0.0012, (2) 0.0021, (3) 0.0048, (4) 0.0076, (5) 0.0116(6) 0.0167, and the effective rate constant k_{eff}: (1) 0.0178, (2) 0.0312, (3) 0.0714, (4) 0.1131, (5) 0.1726, (6) 0.2484

In order to investigate influence of incident light intensity on regeneration kinetics, we performed feedback current distance curve measurement at a fixed concentration of electrolyte. Figure 3 shows the effective rate constant k_{eff} for P1 dye in T^- electrolyte and I^- electrolyte as a function of photon density, J_{hv} in different LEDs: (a) for blue LED and (b) for red LED. It was found with a blue LED, the k_{eff} for P1 dye in 1 mM T^- electrolyte increased from 0.355×10^{-3} to 1.142×10^{-3} cm s^{-1} as J_{hv} increased from 2.2×10^{-9} to 22.4×10^{-9} mol cm^{-2} s^{-1} (○). The k_{eff} for P1 dye in 1 mM I^- electrolyte increased from 0.216×10^{-3} to 0.671×10^{-3} cm s^{-1} (Δ) (Figure 3a and Table1). Figure 3b shows similar observation in k_{eff} for P1 dye-sensitized with red LED. The k_{eff} increased from 0.319×10^{-3} to 0.941×10^{-3} cm s^{-1} (Δ) as the J_{hv} increased from 4.19×10^{-9} to 14.68×10^{-9} mol cm^{-2} s^- in 1 mM I^- electrolyte, while they increased from 0.381×10^{-3} to 1.401×10^{-3} cm s^{-1} (○) in 1 mM T^- electrolyte (Figure 3b and Table 1). This confirms that the effective rate constant k_{eff} of P1 dye with T^- electrolyte is significantly higher than I^- electrolyte.

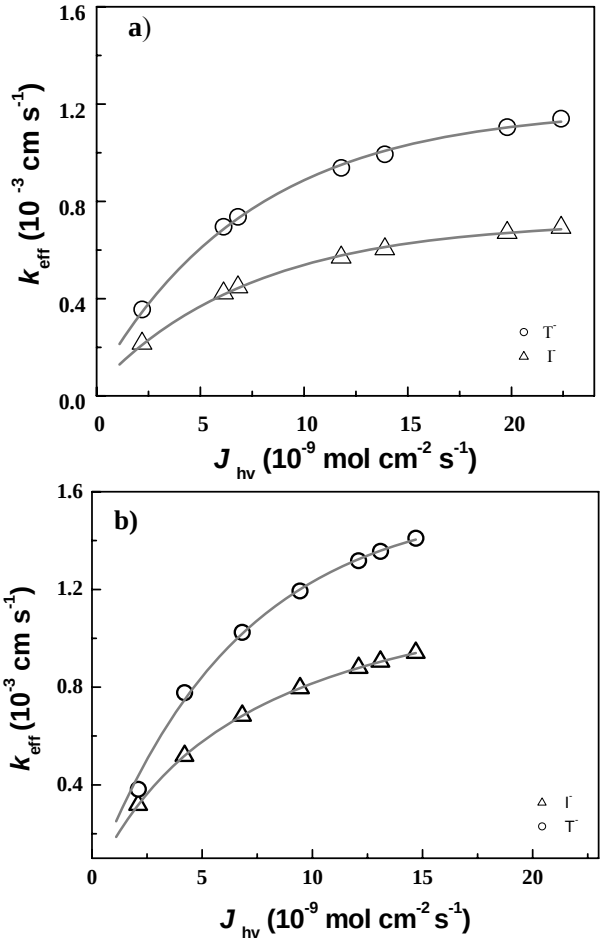

Fig. 3 Plot of experimental values of k_{eff} as a function of J_{hv} (λ). The lines represent fits of k_{eff} according to Eq. 3 with k_{ed} and J_{hv} (λ) as adjustable parameters for T^- electrolyte (○) and I^- electrolyte (Δ) illuminated with (a) blue LED and (b) red LED.

Therefore, the reduction constant k_{red} for regeneration of excited dye and the excitation cross-section (Φ_{hv}) of the adsorbed dye was evaluated by using Eq. 4, exhibiting significant relationship with electrolytes and irradiation intensity. The calculated reduction constant k_{red} for P1 were 3.53×10^5 and 9.67×10^5 mol^{-1} cm^3 s^{-1} in I^- and T^- electrolytes, respectively. The values of Φ_{hv} for P1 dye were calculated to be 9.02×10^{-5} and 1.79×10^{-5} cm^2 mol^{-1} in I^- electrolyte illuminated with blue and red LEDs. The values of Φ_{hv} for P1 dye were 1.28×10^{-4} and 1.23×10^{-5} cm^2 mol^{-1} in T^- electrolyte illuminated with blue and red LEDs, respectively. This result could be attributed to the remarkable dependence of heterogeneous rate constant of dye regeneration on wavelength and intensity.[46,47]

Table 1 Normalized apparent heterogeneous first-order rate constants κ and apparent heterogeneous rate constants (k_{ef}=κ_D/r_T) obtained for the reduction of photo-excited P1 (r_T= 12.5μm, RG=10, $D(T^-)$= 1.35×10^{-5} cm^2 s^{-1}, and $D(I^-)$=1.86×10^{-5} cm^2 s^{-1})

J_{hv} [10^{-9} mol cm^{-2} s^{-1}]	$k_{eff}(T^-)$[10^{-3} cm s^{-1}]	$k_{eff}(I^-)$[10^{-3} cm s^{-1}]
(a) blue LED		
2.2	0.216	0.202
6.1	0.695	0.422
11.8	0.735	0.446
13.9	0.937	0.569
19.8	0.993	0.604
22.4	1.142	0.671
(b) red LED		
4.19	0.381	0.319
6.81	0.777	0.519
9.41	1.025	0.683
12.06	1.193	0.709
13.11	1.317	0.904
14.68	1.401	0.941

Based on above observation, SECM investigation dye-regeneration kinetics of dye with different anchoring group was further carried out in order to understand influence of dye natures. Figure 4 shows the normalized current distance curves and corresponding fitting data for (a) CW1 dye and (b) CW2 dye sensitised NiO films. Under illumination with blue LED for CW1 sensitized NiO film in 1 mM I^-, k_{eff} was increased from 0.014×10^{-3} to 0.171×10^{-3} cms^{-1} as the photon flux of blue LED from 2.2×10^{-9} to 22.4×10^{-9} mol cm^2 s^{-1}. For red LED of photon density increased from 4.19×10^{-9} to 14.68×10^{-9} mol cm^2 s^{-1}, the k_{eff} increased from 0.265×10^{-3} to 0.782×10^{-3} cm s^{-1} for CW1. In same pattern for CW2-senstized NiO films, the k_{eff} increased from 0.145×10^{-3} to 0.182×10^{-3} cm s^{-1} with blue LED and k_{eff} increased from 0.167×10^{-3} to 0.492×10^{-3} cm s^{-1} with red LED (see Table 2).

Table 2 Normalized apparent heterogeneous first-order rate constants κ and apparent heterogeneous first-order rate constants (k_{eff}=κD/r_T) obtained for the reduction of photo-excited CW2, CW1, and P1 by I^- for different illumination intensity of blue, and red LEDs. [I^-]=1mM, D=$1.867\times10^{-5}$$cm^2$ s^{-1}, r_T=12.5μm, RG= 10.

J_{hv} [10^{-9} mol cm^{-2} s^{-1}]	CW2 k_{eff}[10^{-3} cm s^{-1}]	CW1 k_{eff}[10^{-3} cm s^{-1}]	P1 k_{eff} [10^{-3} cm s^{-1}]
(a) blue LED			
2.2	0.145	0.014	0.202
6.1	0.148	0.111	0.422
11.8	0.155	0.141	0.446
13.9	0.162	0.149	0.569
19.8	0.171	0.166	0.604
22.4	0.182	0.171	0.671
(b) Red LED			
4.19	0.167	0.265	0.319
6.81	0.271	0.431	0.519
9.44	0.358	0.568	0.683
12.06	0.417	0.662	0.709
13.11	0.461	0.731	0.904
14.68	0.492	0.782	0.941

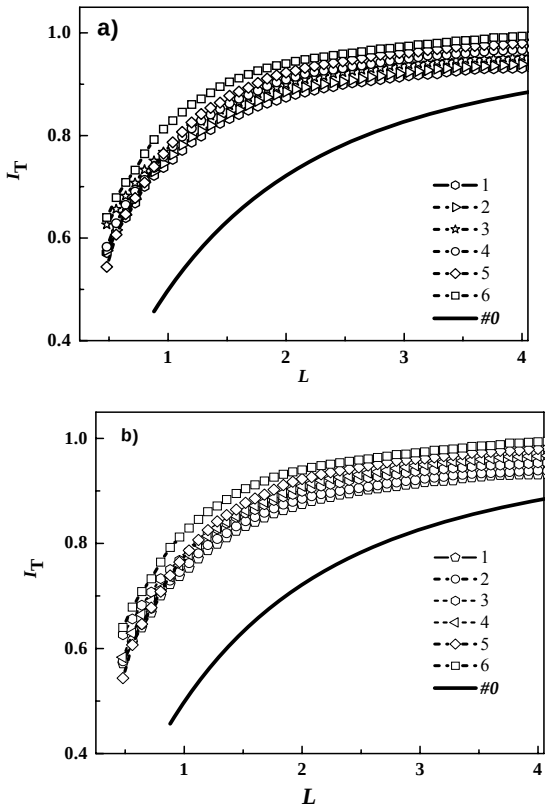

Fig. 4 (a) Comparison of normalized SECM approach curves between Normalized SECM feedback approach curves for the approach of a Pt disk UME towards a NiO/CW1 and NiO/CW2 film in the dark (curve 1) and under illumination by blue LED. Photon flux density of LED in 10^{-9} mol cm^{-2} s^{-1} (a) NiO/CW2 (1) 2.2, (2) 6.1, (3)11.8, (4) 13.9, (5) 19.8, (6) 22.4; V_T = 0.05Vs^{-1}, E_T = 0.7 V, [I^-]=1 mM. k_{eff} × 10^{-3} (1) 0.145, (2) 0.148, (3) 0.155, (4) 0.162 (5) 0.171 (6) 0.182 (b) NiO/CW1, k_{eff} × 10^{-3} (1) 0.014, (2) 0.111, (3) 0.141 (4) 0.149, (5) 0.166, (6) 0.171.

The influence of light intensities on dye regeneration kinetics was compared for CW1, CW2, and P1 dyes (Table 2). The experimental result clearly shows that k_{eff} increases with light intensity. Figure 5 shows the fitting result of k_{eff} vs. J_{hv} varied light intensity of the three dyes in I^- electrolyte as a function of photon flux density J_{hv} with (a) blue and (b) red illumination. It was found that under a given photon flux intensity, the P1 dye have highest k_{eff} values among the three dyes. Under illuminated with blue LED, the k_{eff} values were slightly smaller than those with red LED.The CW1 and CW2 dyes presented more or less the same regeneration kinetics rate constant k_{eff}. It was also observed that the dye with carboxylic acid anchoring group showed faster regeneration process than that of dye with pyridine as anchoring group. This result indicates that the dye regeneration is dependent on dye molecular structure. The values of Φ_{hv} were extracted from the fitting result with Eq. 4 to be 4.51×10^{-5} and 1.06×10^{-5} cm^2 mol^{-1} for CW2 dye illuminated with blue and red LEDs. For CW1 dye Φ_{hv} was calculated to be 3.35×10^{-5} and 2.23×10^{-5} cm^2 mol^{-1} for blue and red LEDs (see Table 3).

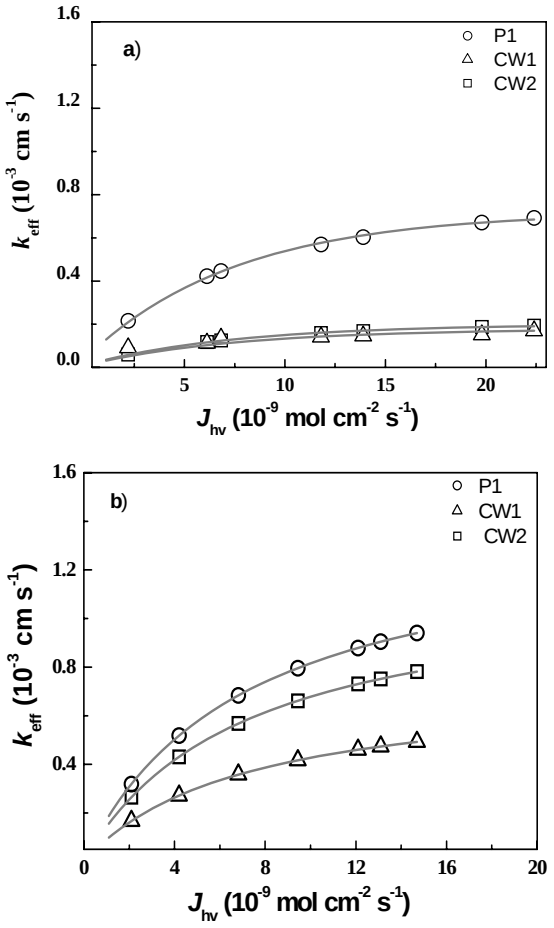

Fig. 5 Plot of experimental values of k_{eff} versus $J_{hv}(\lambda)$: (a) for blue and (b) red LEDs. The lines represent fits of k_{eff} according to Eq. (3) with k_{red} and $\Phi hv(\lambda)$ as adjustable parameters of P1 (○) , CW2 (Δ), and CW1 (□) dyes.

The SCEM investigation of dye regeneration conforms that change of regeneration parameters k, k_{eff}, and k_{red} exhibit significant relationship with incident light intensities. In DSSCs, kinetics of electron transfer reaction at the dye sensitized semiconductor/electrolyte interfaces is critical to device efficiency. Previous report on the P1, CW1 and CW2 dyes revealed their oxidation potential (E_{ox}) at 1.38, 1.179, and 1.109 V (vs. NHE), respectively.[39] The redox potential values of I_3^-/I^- and T_2/T^- were about 0.35 and 0.5 V (vs. NHE). In our experimental observation, the $E(D/D^-)$ were estimated to be -3.13 eV for P1 dye, -3.12 eV for CW1, and -3.09 eV for CW2 (Figure 6). Therefore, the regeneration energy of (ΔG_{reg}) per the elementary charge can be 2.13 eV for P1 dye, 2.3 eV for CW1 dye, and 2.27 eV for CW2. [11, 27, 39] As discussed above, it is significant that the dye regeneration is faster in (T^-) electrolyte compared to (I^-) electrolyte, even though the driving force is smaller than former. Therefore, there is a significant driving force for dye regeneration reaction as illustrated in Figure 6.

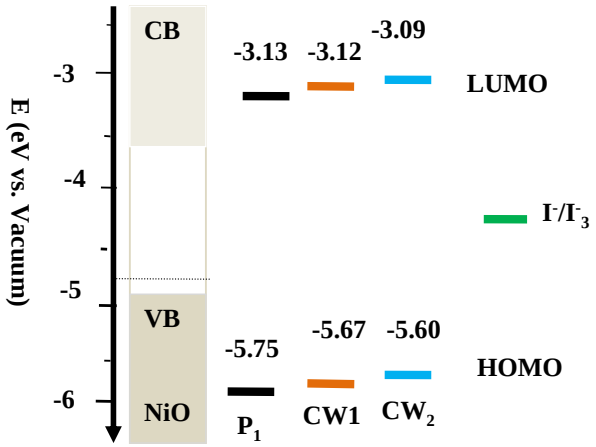

Fig. 6 Schematic energy level diagram for various dyes with respect to the NiO.

Table 3 Fitting results of the reduction rate constant k_{red} and cross section Φ_{hv} for three organic dyes from the experimental data of k_{eff}, I^- electrolyte concentration.

Dye	LED	k_{red} [mol^{-1} cm^3 s^{-1}]	Φ_{hv} [$mol^{-1}cm^2$]
P1	Blue	3.53×10^6	4.53×10^{-5}
	Red		2.21×10^{-5}
CW1	Blue	3.72×10^5	1.15×10^{-5}
	Red		2.23×10^{-5}
CW2	Blue	9.95×10^5	3.35×10^{-5}
	Red		1.06×10^{-5}

Table 4 Fitting results of the reduction rate constant k_{red} and cross section Φ_{hv} for P1 dye in different electrolytes.

Electrolyte	LED	k_{red} [mol^{-1} cm^3 s^{-1}]	Φ_{hv} [$mol^{-1}cm^2$]
I-	Blue	3.53×10^6	4.53×10^{-5}
	Red		2.21×10^{-5}
T-	Blue	9.67×10^6	1.28×10^{-4}
	Red		1.23×10^{-5}

Conclusion

The SECM with feedback mode can provide insight on impact of different parameters on dye regeneration process, including dye molecular structure and redox couples. The experimental results in this study showed that the dye-regeneration rate constant k_{red} for the organic D-π-A dye P1 was about 3.53×10^6 mol^{-1} cm^3 s^{-1} with an excitation cross section about 4.53×10^{-5} cm^2 mol^{-1} (blue illumination) with the standard I^- electrolyte. The dye regeneration process can be boosted by using thiolate-based electrolyte, showing k_{red} of 9.67×10^6 mol^{-1} cm^3 s^{-1} with an excitation cross section about 1.28×10^{-4} mol^{-1} cm^2. Changing the carboxylic acid anchoring group with pyridine for CW1 and CW2 dyes, the dye regeneration rate constant of k_{red} were determined to be 3.72×10^5 and 9.95×10^5 mol^{-1} cm^3 s^{-1}, the excitation cross section to be 1.15×10^{-5} and 3.35×10^{-5} cm^2 mol^{-1}, respectively. The observed difference is related to electrolyte composition, the internal structure of

sensitizers, and the intermolecular interaction of dye and electrolyte. The molecular structure dependence of dye-regeneration process can be attributed to the drive force for the charge transfer reaction. Therefore, SECM measurement allows for rather straight forward test of different electrolyte compositions on the same substrate without the need to construct series of complete cells. This method contributes to selection and design of high efficient electrolytes and sensitizers for improvement p-type DSSC.

Acknowledgements

We gratefully acknowledge the 973 Program of China (2014CB643506, 2013CB922104, and 2011CBA00703), NSFC (21103578, 21161160445, and 201173091), and and the CME with the Program of New Century Excellent Talents in University (NCET-10-0416). The authors thank the Analytical and Testing Center of Huazhong University of Science and Technology for support.

Notes and references

Wuhan National Laboratory for Optoelectronics, School of Optical and Electronic Information, Huazhong University of Science and Technology, 1037 Luoyu Road, Wuhan 430074 (P. R. China). E-mail: mingkui.wang@mail.hust.edu.cn, ciac_sheny@mail.hust.edu.cn

† Electronic Supplementary Information (ESI) available: [details of any supplementary information available should be included here]. See DOI: 10.1039/b000000x/

1. B. O'Regan, M. Grä tzel, *Nature*, 1991, **353**, 737-740.
2. A. Hagfeldt, G. Boschloo, L. Sun, L. Kloo, H. Pettersson, *Chem. Rev.,* 2010, **110**, 6595-6663.
3. S. Nakade, Y. Makimoto, W. Kubo, T. Kitamura, Y. Wada, *J. Phys. Chem. B*, 2005, **109**, 3488-3493.
4. M. Grätzel, *Acc. Chem. Res.,* 2009, **42**, 1788-1798.
5. S. Rhee, W. Kwon, *J. Chem. Eng.,* 2011, **7**, 1481-1494
6. T. Hamann, R. Jensen, B. Martinson, H. Ryswyk, J. Hoppy, *Energy Environ. Sci.,* 2008, **1**, 66-78.
7. T. Daeneke, A, Mozer, T, Kwon, N. Duffy, A. Holmes, U. Bach, L. Spiccia, *Energy Environ. Sci.*, 2012, **5**, 7090-7099.
8. J. Bandara, H. Weerasinghe, *Sol. Energy Mater. Sol. Cells*, 2005, **85** 385-390.
9. Y. Tachibana, J. Moser, M. Grätzel, D. Klug, J. Durrant. *J. Phys. Chem.*, 1996, **100**, 20056-20062.
10. S. Haque, Y. Tachibana, D. Klug, J. Durrant, *J. Phys. Chem. B* 1998, **102**, 1745-1749
11. E. Gibson, L. Pleux, J. Fortage,Y. Pellegrin, E. Blart, F. Odobel, A. Hagfeldt, G. Boschloo, *Langmuir* 2012, 2**8**, 6485-6493.
12. M. Nazeeruddin, A. Kay, I. Rodicio, R. Baker, E. Mueller, P. Liska, N. Vlachopoulos, M. Grätzel, *J. Am. Chem. Soc.*, 1993, **115**, 6382-6390.
13. P. Wang, S. Zakeeruddin, J. Moser, M. Nazeeruddin, T. Sekiguchi, M. Grätzel, *Nat. Mater.*, 2003, **2**, 402-407.
14. A. Yella, H. Lee, H. Tsao, C. Yi, A. Chandiran, M. Nazeeruddin, E. Diau, C. Yeh, S. Nazeeruddin, M. Grätzel, *Science*, 2011, **334**, 629-634.
15. X. Xu, B. Zhang, J. Cui, D. Xiong, Y. Shen, W. Chen, L. Sun, Y. Cheng, M. Wang, *Nanoscale*, 2013, **5**, 7963-7969.
16. X. Xu, J. Cui, J. Han, J. Zhang, Y. Zhang, L. Luan, G. Alemu, Z. Wang, Y. Shen, D. Xiong, W. Chen, Z. Wei, S. Yang, B. Hu, Y. Cheng, M. Wang, *Sci. Rep.*, 2014, *4*, 3961.
17. Z. Xu, D. Xiong, H. Wang, W. Zhang, X. Zeng, L. Ming, W. Chen, X. Xu, J. Cui, M. Wang, S. Powar, U. Bach, Y. Cheng, *J. Mater. Chem. A*, 2014, *2*, 2968-2976.
18. F. Odobela, Y.Pellegrin, E. Gibsonb, A. Hagfeldtc, A. Smeig, L. Hammarström, *Coord. Chem. Rev.*, 2012, **256**, 2414-2423.
19. F. Odobel, L. Pleux, Y. Pellegrin, E. Blart, *Acc. Chem. Res.*, 2010, **43** 1063-107.
20. J. He, H. Lindstrom, A. Hagfeldt, S. Lindquist, *J. Phys. Chem. B* 1999, **103**, 8940- 8943.
21. A. Nattestad, M. Ferguson, R. Kerr, Y. Cheng, U. Bach, *Nanotechnology* 2008, **19**, 295304-295313
22. S. Sumikura, S. Mori, S. Shimizu, H. Usami, E. Suzuki, *Photochemical. Photobiol. A Chem.* 2008, **194**, 143-147.
23. C. Fernando, A. Kitagawa, M. Suzuki, K. Takahashi, T. Komura, *Sol. Energy Mater. Sol. Cells*, 1994, **33**, 301-315.
24. L. Li, E. Gibson, P. Gibson, G. Qin, M. Boschloo, A. Gorlov, L. Hagfeldt, L. Sun, *Adv. Mater.*, 2010, **22**, 1759-1762.
25. X. Wu, G. Xing, L. Tan, Y. Webster, T. Sum, K. Edwin, *Phys. Chem. Chem. Phys.* 2012, **14**, 9511-9519
26. X. Zhang, F. Huang, A. Nattestad, K. Wang, D. Fu, A. Mishra, P. Bäuerle, U. Bach, Y. Cheng. *Chem. Commun.*, 2011, **47**, 4808-4810.
27. P. Qin, M .Linder, T. Brinck, G. Boschloo, A. Hagfeldt, L. Sun, *Adv. Mater.*, 2009, **21**, 2993-2996
28. M. Griffith, K. Sunahara, A. Furube, A, Mozer, L. David, P. Wagner, G. Wallace, S. Mori, *J. Phys. Chem. C*, 2013, **117**, 1885-1889
29. P. Qin, J. Wiberg, E. Gibson, M. Linder, L. Li, T. Brinck, A. Hagfeldt, B. Albinsson, L. Sun, *J. Phys. Chem. C* 2010, **114**, 4738-4748.
30. S. Ito, T. Murakami, P. Comte, P. Liska, C. Grätzel, M. Nazeeruddin; M. Grätzel, *Thin Solid Films*, 2008, **516**, 4613-4619.
31. G. Wittstock, M. Burchardt, S. Pust, Y. Shen, C. Zhao, *Angew. Chem. Int. Ed.* 2007, **46**, 1584-1617.
32. P. Sun Franc, O. Laforge, M. Mirkin, *Phys. Chem. Chem. Phys.* 2007, **9**, 802- 823.
33. J. Amphlett, G. Denuault, *J. Phys. Chem. B*, 1998, **102**, 9946- 9951.
34. C. Wei, A. Bard, *J. Phys. Chem.* 1995, **99**, 16033-16042.
35. Y. Shao, M. Mirkin, *J. Phys. Chem. B*, 1998, **102**, 9915-9921.
36. Y. Shen, K. Nonomura, D. Schlettwein, C. Zhao, G. Wittstock, *Chem. Eur. J.* , 2006, **12**, 5832-5839.
37. Y. Shen, U. Tefashe, K. Nonomura, T. Lowenstein, D. Schlettwein, G. Wittstock, *Electrochemical Acta*, 2009, **55**, 458-464.
38. B. Zhang, X. Xu, X. Zhang, D. Huang, S. Li, Y. Zhang, F. Zhan, M. Deng, Y. He, W. Chen, Y. Shen, M. Wang, *ChemPhysChem*, 2014, DOI: 10.1002/cphc.201301076.
39. J. Cui, J. Lu, X. Xu, K. Cao, Z. Wang, G. Alemu, H. Yuang, Y. Shen, J. Xu, Y. Cheng, M. Wang. *J. Phys. Chem. C,* **2014**, 118, 16433-16440.
40. L. Lu, J. Bai, X. Xu, Z. Li, K. Cao, J. Cui, M. Wang, *Chin. Sci. Bull.*, 2012, **57**, 4131-4142.
41. M. Wang, C. Grätzel,S. Zakeer, M. Grätzel, *Energy Environ. Sci.*, 2012, **5**, 9394-9405.
42. M. Wang, N. Chamberland, L. Breau, J. Moser, R. Humphry-Baker, B. Marsan, S. Zakeeruddin, M. Grätze, *Nat. Chem.* 2010, **2**, 385-389.
43. X. Zhang, F. Huang, A. Nattestad, K. Wang, D. Fu, A. Mishra, P. Bäuerle, U. Bach, Y. Cheng, *Chem. Commun.*, 2011, **47**, 4808-4810.
44. X. Zhang, Z. Zhang, D. Chen, P. Bauerle, U. Bach, Y. Cheng, *Chem. Commun.*, 2012, **48**, 9885-9887.
45. S. Ito, T. Murakami1, P. Comte, P. Liska, C. Grätzel, M. Nazeeruddin, M. Grätzel, *Thin Solid Films*, 2008, **516**, 4613–4619
46. S. Powar, T. Daeneke, M. Ma, D. Fu, N. Duffy, G. Gçtz, M. Weidelener, P. Bauerle, L. Spiccia, U. Bach, *Angew. Chem. Int. Ed.*, 2013, **52**, 602-605.
47. G. Alemu, B. Zhang, J. Li, X. Xu, J. Cui, Y. Shen, M. Wang, *Nano*, 2014, **09**, 1440008.